

This work was written as part of one of the author's official duties as an Employee of the United States Government and is therefore a work of the United States Government. In accordance with 17 U.S.C. 105, no copyright protection is available for such works under U.S. Law.

Public Domain Mark 1.0

<https://creativecommons.org/publicdomain/mark/1.0/>

Access to this work was provided by the University of Maryland, Baltimore County (UMBC) ScholarWorks@UMBC digital repository on the Maryland Shared Open Access (MD-SOAR) platform.

Please provide feedback

Please support the ScholarWorks@UMBC repository by emailing scholarworks-group@umbc.edu and telling us what having access to this work means to you and why it's important to you. Thank you.

A heuristic approach to global landslide susceptibility mapping

Thomas Stanley^{1,2,3}  · Dalia B. Kirschbaum³

Received: 6 July 2016 / Accepted: 19 January 2017 / Published online: 7 February 2017
© Springer Science+Business Media Dordrecht (outside the USA) 2017

Abstract Landslides can have significant and pervasive impacts to life and property around the world. Several attempts have been made to predict the geographic distribution of landslide activity at continental and global scales. These efforts shared common traits such as resolution, modeling approach, and explanatory variables. The lessons learned from prior research have been applied to build a new global susceptibility map from existing and previously unavailable data. Data on slope, faults, geology, forest loss, and road networks were combined using a heuristic fuzzy approach. The map was evaluated with a Global Landslide Catalog developed at the National Aeronautics and Space Administration, as well as several local landslide inventories. Comparisons to similar susceptibility maps suggest that the subjective methods commonly used at this scale are, for the most part, reproducible. However, comparisons of landslide susceptibility across spatial scales must take into account the susceptibility of the local subset relative to the larger study area. The new global landslide susceptibility map is intended for use in disaster planning, situational awareness, and for incorporation into global decision support systems.

Keywords Landslide · Landslide susceptibility · Remote sensing · GIS · Fuzzy logic

1 Introduction

Landslides cause thousands of fatalities annually (Petley 2012; Kirschbaum et al. 2015b; Haque et al. 2016), as well as substantial property damage. The true risk may be higher than that observed in recent landslide catalogs due to the fact that most casualties are caused by

✉ Dalia B. Kirschbaum
dalia.b.kirschbaum@nasa.gov

¹ Universities Space Research Association, Columbia, MD, USA

² Goddard Earth Sciences Technology and Research, Columbia, MD, USA

³ Hydrological Sciences Laboratory, NASA Goddard Space Flight Center, 8800 Greenbelt Road, Greenbelt, MD 20771, USA

rare catastrophic events (Petley et al. 2005). The first step in characterizing the potential impact of landslides (defined in this paper as any mass movements, including shallow debris flows, rock falls, and deep-seated rotational slides) is to identify where these events have occurred in the past. An ideal landslide inventory would provide both spatial and temporal information on all previous landslides over a certain domain. However, most inventories are limited to a short time period that may not fully reflect the probability of catastrophic landslides. In addition, many landslides go unreported. Therefore, it is helpful to consider not only the historical record of landslide occurrences, but also account for general principles of slope stability when predicting the spatial patterns of future landslide events.

Small-scale (defined in this paper as less than 1:1,000,000 scale) landslide susceptibility maps suffer from four main problems: (1) the lack of comprehensive and unbiased landslide inventories; (2) the coarse resolution or absence of data inputs; (3) regional differences in the importance of causative factors; and (4) the dearth of expertise on landscape processes across a vast region. This work addresses several of these limitations through a heuristic approach to represent relative landslide susceptibility at the global scale.

There have been several projects to represent susceptibility at continental or global scales (Table 1). The landslide overview map of the conterminous USA (Radbruch-Hall et al. 1982) was produced prior to the widespread use of digital elevation models (DEM), an input seen in nearly all later research. The European and Indian maps (BMTPC and CDMM 2003; Günther et al. 2014) represent collective efforts in which multiple local datasets were assembled into a continental view of landslide susceptibility. In contrast, China and the Caribbean region were analyzed as single units (Liu et al. 2013; Kirschbaum et al. 2015a). No variable or method was adopted by all authors. The general trend over time is toward “objective” and away from “subjective” methods. Despite covering vast areas, all but one of the maps were developed with reference to a relatively small landslide inventory for validation. Given this challenge, it is not surprising that most methodologies rely on heuristic methods. Slope and geological classification were used most often, while land cover and seismicity were each used in half the studies. Classification and ranking of slope data was fairly consistent among the studies. This work adopts the standard of practice in previous research at continental and global scales and applies it to previously unavailable datasets with a flexible fuzzy method. The resulting landslide susceptibility map forms one component of a global decision support system that identifies landslide potential in nearly real time, in concert with satellite-based precipitation estimates.

2 Data

In previous studies (Table 1), slope, geology, land cover, and tectonic features were used most frequently to develop most of the small-scale landslide susceptibility maps. The same variables were considered in the current work, but with different data sources (Table 2). Information on roads was also incorporated due to the association between roads and increased landslide rates (Larsen and Parks 1997; Petley et al. 2007; Kirschbaum et al. 2015b). Global or nearly global data is available for all of these variables, often without charge.

2.1 Topography

There are relatively few sources of topographic information with global coverage. One of the best is the Shuttle Radar Topography Mission (SRTM). This dataset was initially

Table 1 Summary of selected landslide susceptibility maps

Study area	USA	USA	Europe	India	China	Indonesia	Caribbean	World	World	Total
Reference	Radbruch-Hall et al. (1982)	Brabb et al. (1999)	Günther et al. (2014)	BMTPC and CDMM (2003)	Liu et al. (2013)	Cepeda (2010)	Kirschbaum et al. (2015a)	Nadim et al. (2006)	Hong et al. (2007)	
Landslide events	Unknown	24,000	102,000	10	1200	97	318	3000	555	
Resolution (m)	N/A	950	1000	N/A	1000	1000	1000	1000	27,800	
Methodology	Expert opinion	Expert opinion	Analytical process & Frequency ratio	Weighted linear combination	Neural network	Weighted linear combination	Fuzzy overlay	Weighted linear combination	Weighted linear combination	
Slope		X	X	X	X	X	X	X	X	8
Aspect					X					1
Curvature					X					1
Relief			X							1
Elevation					X				X	2
Geology	X		X	X	X	X		X		6
Geomorphological classification				X						1
Soil type or texture					X		X		X	3
Soil moisture						X		X		2
Land cover/NDVI			X	X	X	X		X	X	5
Distance to stream/Drainage density					X				X	2
Köppen climate classification			X							1
Seismicity				X	X	X	X	X		5
Precipitation				X		X		X		3
Road presence							X			1

In general, previous researchers used heuristic methods to produce maps with resolutions of approximately 1 km (30 arc seconds). Some variables, such as slope and geology, were commonly used, and represent a rough consensus on the importance of these factors

Table 2 Global landslide susceptibility map was created by combining information from four principal sources of information for five explanatory variables: slope, distance to fault, geological classification, presence of roads, and forest loss

Data type	Data set	Resolution/accuracy	Explanatory variable	Extent	Source and details
Elevation	Viewfinder panoramas digital elevation data	3 arc seconds (~90 m)	Slope	84°N–72°S	de Ferranti (2014a) derived from 3 arc seconds SRTM DEM and several other sources.
Faults and geologic regions	Geological map of the world, 3rd edition	1:50,000,000	Distance to fault zones and geological classification	Global	Bouysse (2009)
Roads	Openstreetmap	Variable	Presence of roads	Global	OpenStreetMap contributors (2015) Data represents OSM on June 4th, 2015
Forest cover	Global forest change 2000–2013	30 m/99.6%	Forest loss	80°N–60°S	Hansen et al. (2013)

released at a 3 arc seconds (approximately 30 m) resolution (Rabus et al. 2003), but has been released recently at a resolution of 1 arc seconds (approximately 30 m) and is available from 60° North to 56° South. Unfortunately, the Middle East was not available at this resolution at the time of writing. SRTM data contain substantial voids. Several attempts to address this problem have been made, including the SRTM 90 m Digital Elevation Database v4.1 (Jarvis et al. 2008), Global Land Survey Digital Elevation Model (USGS 2008) and HydroSHEDS (Lehner et al. 2008). While many of the SRTM void-filling techniques produce reasonably accurate elevations in flat areas, slope and other elevation derivatives can be severely affected—especially in mountainous terrain. Each product was evaluated by calculating slope over test areas in the Himalayas and the Sahara (where SRTM voids are common). The best global DEM for the purpose of calculating slope in complex topography was found to be Viewfinder Panoramas (de Ferranti 2014a). This is attributed to the use of several sources of topographic information in addition to SRTM, which are described below.

In order to better represent the size and shape of complex topographic features, de Ferranti (2014a) reviewed multiple series of topographic maps, as well as data from SRTM, the Advanced Spaceborne Thermal Emission and Reflection Radiometer (Hirano et al. 2003), the Ice, Cloud, and land Elevation Satellite (Schutz et al. 2005), and the RADARSAT Antarctic Mapping Project (Jezek 2002). Landsat imagery was also consulted. Then these data sources were combined in a manner designed to draw on the advantages of each (de Ferranti 2014b). Typically, SRTM DEM 1-degree tiles with 3 arc seconds resolution formed the basis for the map. Voids in each tile were filled by the most accurate alternative source. The first step in filling voids was to calculate topographic contours from the SRTM DEM. Next, the contours were connected across the no-data regions by referencing topographic maps, including spot heights. Then the map was searched for artifacts, which were corrected by hand. Finally, the contours were converted back to a raster DEM. In some cases, voids were filled directly with

data from the ASTER Global DEM (GDEM) and then checked for artifacts. In Europe, most elevations are based on topographic maps or more precise sources, rather than SRTM data. Unfortunately, the tile-based contouring process seems to have introduced errors along some tile edges. The specific reason for this behavior is unclear, and the global effect is relatively minor, but it should be noted. Nevertheless, this process produces a global DEM with far better representation of SRTM no-data regions than other free elevation datasets.

DEM tiles from Viewfinder Panoramas were converted to slope with R’s raster package (Hijmans 2015), and then slopes were aggregated to the output resolution by selecting the maximum slope value from the collection of pixels. Maximum slope was chosen to represent the most extreme conditions within each pixel and to ensure that the map identifies all possibly susceptible areas within the cell. Finally, all tiles were merged into a single map. This slope map resembles the global slope dataset for estimation of landslide occurrence resulting from earthquakes (Verdin et al. 2007), but with the advantage of increased accuracy at high elevations. In addition, the new slope map improved the representation of coastal terrain, which should aid decision-making in the British Isles and other locations where coastal bluff collapse is a major hazard (Fig. 1). However, comparison of the slope datasets revealed less than one degree of difference for most locations.

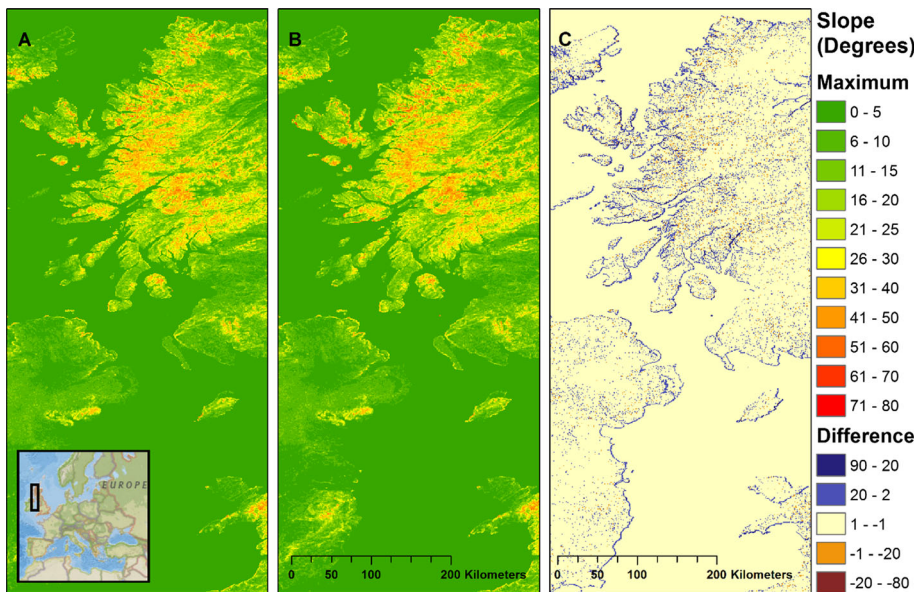


Fig. 1 Coastline of the Irish Sea and Scottish Highlands as modeled by **a** the maximum values from the 30 arc seconds global slope dataset for estimation of landslide occurrence resulting from earthquakes, **b** the maximum slopes aggregated from the Viewfinder Panoramas DEM, **c** to determine the relationship between these layers, the global slope dataset was subtracted from the new slope map. *Purple* indicates higher slopes in the new dataset. *Brown* indicates locations where the global slope dataset is steeper. Slope values are nearly identical (*off-white*) in most locations. The primary difference is the inclusion of many coastal pixels in the newer map. This probably results from the application of a restrictive land mask to elevation data prior to production of the global slope dataset. Since many landslides in the UK and around the world occur at coastal bluffs, inclusion of these pixels may help to balance the concerns of interior and maritime regions

2.2 Geology

Many previous susceptibility mapping efforts include soil and/or rock types as explanatory variables, since each material has a unique strength, permeability, and stress history. Unfortunately, most geotechnical properties are not available on a global basis. In order to represent this factor, the Geological Map of the World (GMW) (Bouysse 2009) was simplified into the five categories described by Nadim et al. (2006) and converted to a raster file with a resolution of 30 arc seconds (Table 3). The rating was rescaled between 0 and 1 for consistency with other model inputs. The rationale for these ratings was that younger rocks tend to be less consolidated than older rocks, and for any given age, sedimentary rocks tend to be weaker than Igneous and Metamorphic rocks. Nadim et al. also pointed out that even though lava rocks may be strong, volcanic deposits are often made of interbedded weak materials. In addition, chemical weathering and alteration often have a strong effect on volcanic materials, leaving landslide-prone soils and rocks (Frolova et al. 2015; Reid et al. 2001).

2.3 Seismicity

Seismicity increases landslide hazard by destabilizing the soil and debris on slopes, introducing additional fracturing that can allow water to penetrate and more rapidly influence the subsurface, and creating steeper or more marginal slopes as a result of seismic shaking and co-seismically triggered landslides (Keefer 1994; Okamoto et al. 2013). In addition, tectonically active areas may be prone to increased erosion, due to jointing, graben formation, volcanism, stresses (Scheidegger and Ai 1986), and uplift (Larsen and Montgomery 2012). To describe these effects, vector representations of major faults were obtained from the GMW. The distance to these faults was calculated to create a proxy for tectonic activity.

Table 3 Lithological classification

Material, age	Rating (Nadim et al. 2006)	Rescaled rating
Water bodies	Null	0.1
Greenland ice cap	Unknown	0.1
Extrusive volcanic rocks, Archean–Paleozoic	1	0.2
Endogenous rocks, Archean–Paleozoic	1	0.2
Old sedimentary rocks, Archean–Paleozoic	2	0.4
Extrusive volcanic rocks, Paleozoic–Mesozoic	2	0.4
Endogenous rocks, Paleozoic–Mesozoic	2	0.4
Sedimentary rocks, Paleozoic–Mesozoic	3	0.6
Extrusive volcanic rocks, Mesozoic	3	0.6
Endogenous rocks, Mesozoic–Cenozoic	3	0.6
Sedimentary rocks, Paleozoic–Mesozoic	4	0.8
Extrusive volcanic rocks, Mesozoic–Cenozoic	4	0.8
Extrusive volcanic rocks, Cenozoic	5	1.0

2.4 Forest loss

Land use is commonly used to explain patterns in landslide susceptibility (Korup and Stolle 2014). However, the association between specific land cover classes and the probability of landslides is challenging to characterize globally. While ontological difficulties may be avoided by use of a single global dataset, some error is likely introduced by grouping disparate biota into a relatively small number of classes. More importantly, there has not been clear consensus from the research community as to how to weight these classes. Most studies assign high susceptibility to urban areas and low susceptibility to forested areas, which might reflect the impact of anthropogenic disturbances on slope stability but could also reflect a bias toward urban areas in landslide inventories. The relationship between landslide initiation and land cover classes is more ambiguous. Empirically fitted weights would seem to obviate a research review, but biases in landslide inventories can generate incorrect associations between specific land cover classes (Steger et al. 2016b), as well as support a false sense of confidence in the resulting model (Steger et al. 2016a). Finally, it should be noted that land cover is a constantly changing variable (van Westen et al. 2008). The changes caused by fires, urbanization, etc. are likely to have more predictive power than the static land cover class itself. For these reasons, land use/land cover was eschewed in favor of forest loss.

Vegetation contributes to slope stability by binding soil particles together and enhancing evaporation (Sidle et al. 1985, 2006; Haigh et al. 1995). In a few cases, vegetation may increase hazard, but most slopes are strengthened by the presence of vegetation and weakened by its loss. To represent this variable, a Landsat-based global map of forest loss from 2000 to 2013 was evaluated (Hansen et al. 2013). The 30-m forest loss pixels were aggregated to a resolution of 30-arc seconds by treating the binary output pixel as “forest loss” if it contained any 30-m forest loss pixel. The resulting map represents forest cover change due to many causes, including timber harvesting, fire, and storms.

2.5 Roads

Roads may increase the frequency of mass wasting events (Haigh et al. 1989; Larsen and Parks 1997). Particularly in developing countries, roads built into and along steep mountain terrain often serve to destabilize the slope (similar to a river cut at a slope’s toe), which can increase the frequency of landslides. After visual comparisons with VMAP Level 0 [NIMA (National Imagery and Mapping Agency) 1993] and gROADS (CIESIN and ITOS 2013), the vector dataset OpenStreetMap (OSM) (OpenStreetMap contributors 2015) was selected to represent this factor, due its more comprehensive and accurate coverage. This roadway network was converted to a raster layer at a resolution of 30 arc seconds. Larsen and Parks (1997) observed that landslide scars were far more common within 85 m of roads. While rates remained slightly elevated at greater distances, the effects beyond 100 m from the road were less pronounced. Researchers working at the local scale typically classify distance to road by tens or hundreds of meters when mapping landslide susceptibility (Ayalew and Yamagishi 2005; Weirich and Blesius 2007; Dahal et al. 2008; Regmi et al. 2013; Bhatt et al. 2013; Rubel and Ahmed 2013). With a pixel size of approximately 1 square kilometer, the current susceptibility map cannot model the effect of road construction with the same specificity as local studies. Thus, the raster

representation of road-related hazards was simplified to the presence or absence of a highway in any given pixel.

2.6 Landslide inventories

Landslide inventories from several different events, geographic regions, and methodologies were obtained for validation of the global landslide susceptibility map (Table 4). Of these, only the Global Landslide Catalog (GLC; Kirschbaum et al. 2015b) covers the entire study area. The GLC was compiled from media reports, online disaster databases, and other sources when available, with an emphasis on rainfall-triggered landslides. The database has reports from 2007 to the present. In order to reduce the effects of spatial error on validation statistics, 1194 rainfall-triggered landslides with a spatial accuracy of 1 km or better were selected from a total of 6790 events in the complete GLC. The remaining points could be useful for evaluating products with a coarser resolution, such as landslide susceptibility by state, province or country, but were not used for this analysis. Other inventories were selected to represent different geographic areas and compilation methodologies (Table 4). Some inventories are quite large (Guzzetti et al. 1994; DOGAMI 2015), some cover a long time period (Devoli et al. 2007a; Gerencia de Geología 2012), and some are relatively unbiased but correspond to a single event or observation period (Bucknam et al. 2001; ICIMOD 2010). In every case, the local inventory contains more landslides per square kilometer than the GLC, which indicates substantial underreporting at the global scale. Reporting biases and uncertainty in this catalog have been described in Kirschbaum et al. (2010, 2015b).

Table 4 Landslide inventories used for validation of the landslide susceptibility map

Data set	Number of points/ polygons	Geographic extent	Source
Landslides triggered by Hurricane Mitch	11,555 landslide initiation points	Eastern Guatemala	Bucknam et al. (2001)
Historical landslides in Nicaragua	19,565 points	Nicaragua	Devoli et al. (2007b, a)
Landslide inventory of El Salvador	129 points	El Salvador	Gerencia de Geología (2012)
Landslide maps of Utah	2120 polygons	Utah, USA	Elliott and Harty (2010)
Statewide landslide information database for Oregon, release 3.0 (SLIDO-3.0)	12,095 points	Oregon, USA	DOGAMI (2015)
AVI	12,224 points	Italy	Guzzetti et al. (1994)
Badakhshan province inventory	609 polygons	Badakhshan, Afghanistan	Zhang et al. (2015)
Koshi inventories	3407 polygons	Koshi river basin	ICIMOD (1992, 2010)
GLC	1194 points	Global	Kirschbaum et al. (2015b)

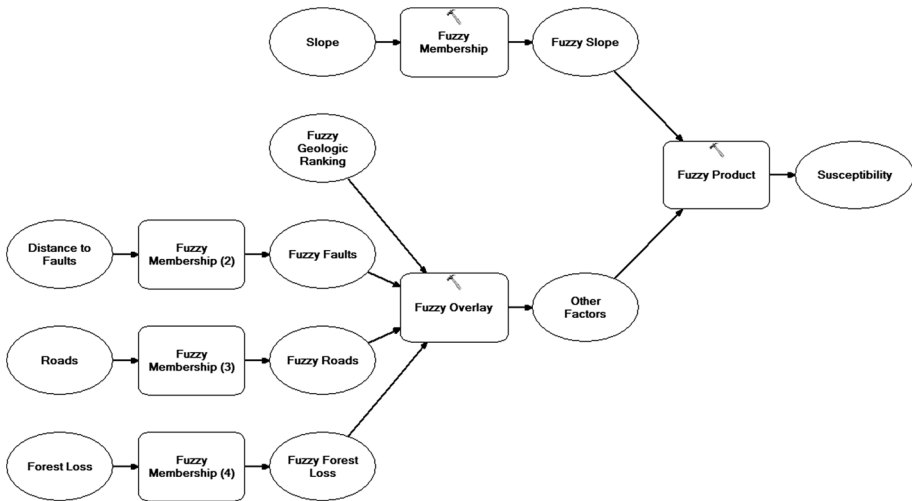


Fig. 2 Fuzzy overlay model combined data on bedrock, faults, forests, and roads with fuzzy gamma operator, where $\gamma = 0.9$. Then slope was introduced with a product function to ensure that no flat ground was identified as highly susceptible. Ovals indicate data, while rectangles with the hammer symbol indicate tools from ArcGIS 10.2 Spatial Analyst

3 Methods

A heuristic fuzzy approach has been taken at the continental (Kirschbaum et al. 2015a), regional (Ahmed et al. 2014), and local scales (Champati ray et al. 2007), but it has not been previously applied at the global scale. Fuzzy landslide models offer some advantages, which include the ability to combine similar datasets in a nested sequence prior to the final combination, the ability to use both continuous and discrete inputs, and widespread integration into GIS software. A disadvantage is that the output is a “possibility,” which is not strictly comparable to the probabilities generated by classical statistics. The heuristic fuzzy approach also enforces transparency, because all of the transformation functions are defined in advance. Unlike some machine-learning models, the hypothesis represented by the fuzzy overlay model must comport with prior knowledge, not just fit the data. This advantage is particularly important for landslide inventories that are known to have significant spatial biases.

Applying fuzzy logic within a GIS requires two distinct steps (Bonham-Carter 1994). In the first step, a fuzzy membership function is assigned for each variable. This function serves to transform the values of the explanatory variable to a range between zero and one. The transformation should reflect the relationship between the variable and landslide susceptibility. For example, slope was assigned the “large” function available in ArcGIS 10.2 (ESRI 2013) to represent the fact that susceptibility grows quickly between 10° and 30° slopes. The second step in fuzzy overlay is to combine the fuzzy membership values with a fuzzy operator such as “fuzzy and” or “fuzzy or.” In this study, all variables other than slope were combined with the fuzzy gamma operator:

$$\mu = \left(1 - \prod_{i=1}^n (1 - \mu_i) \right)^{\gamma} \times \left(\prod_{i=1}^n \mu_i \right)^{1-\gamma} \quad (1)$$

where μ is the possibility that a pixel is susceptible to landslides, n is the number of variables to be combined, μ_i is the possibility that a landslide will occur given the value of the variable i , and γ is the parameter that controls whether μ is closer to the largest or smallest μ_i . In order to determine an appropriate value of gamma, it was varied between 0 to 1 at intervals of 0.1. Each version of the global map was assessed, as described below. Finally, slope was introduced through a product function to ensure that no flat terrain would be given high susceptibility values (Fig. 2). The use of slope gradient as a critical predictor means that the landslide susceptibility map should provide more information on mass movements that require a minimum gradient, such as rock falls and debris flows, than on low-angle movements such as lateral spreads.

In order to aid interpretation of the global landslide susceptibility map, the susceptibility values output by the fuzzy overlay model were classified into five categories: very low, low, moderate, high, and very high. The classes were divided at the following fuzzy susceptibility values: 0.11, 0.49, 0.671, and 0.75. This classification scheme was designed so that each category was twice as large as the next highest, e.g., the very low category contains roughly twice as many pixels as the low category. The decreasing category sizes should enable the user to focus efforts upon the most susceptible areas. While much of the world is somewhat susceptible, only 3% is very highly susceptible. Hazards in this relatively small area may be studied or remediated with greater intensity. Figure 3 shows the proportion of GLC locations in each susceptibility category.

Receiver operating characteristic (ROC) curves are commonly used to evaluate the performance of binary classifiers, i.e., tests that divide inputs into two outcomes (Zweig and Campbell 1993). Since landslide inventories are rarely complete, some locations are likely to contain unreported landslides. This is especially true for the current study area, where landslides have been recorded in less than 1% of the map's pixels. Thus, ROC

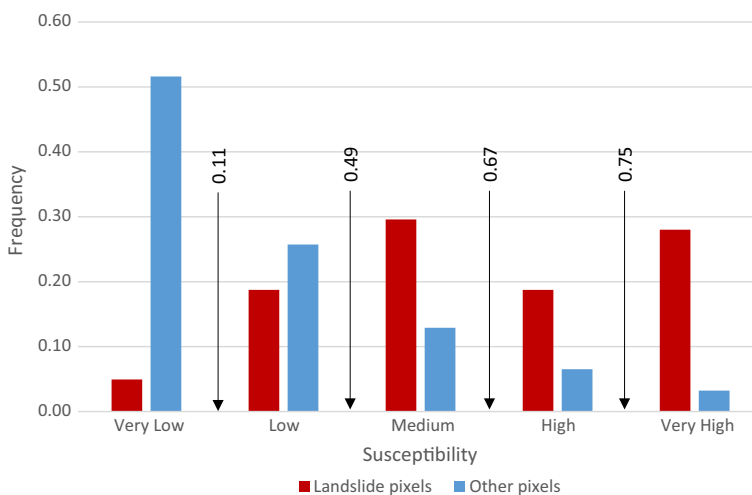


Fig. 3 Distribution of susceptibility for the locations recorded in the GLC (red) and for other areas (blue). The classes were divided at the following fuzzy susceptibility values: 0.11, 0.49, 0.67, 0.75

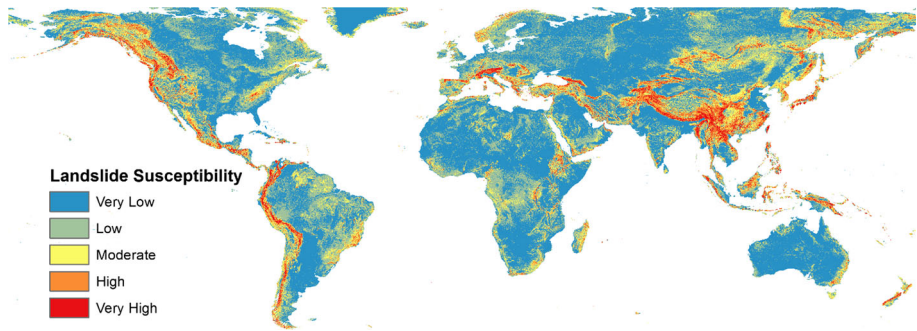


Fig. 4 Global susceptibility map developed using a fuzzy overlay model

analysis will give only a rough guide to map performance, and other aspects of a landslide susceptibility map should also be considered. ROC curves were created for each of the landslide inventories described in Table 4 by calculating the number of historical landslides predicted by each possible susceptibility threshold (true positive rate) and the number of pixels above each susceptibility threshold (false positive rate).

A preliminary ROC analysis indicated that low gamma values generated a susceptibility map with a better fit to the GLC. However, inspection of the resulting maps showed that the low-gamma maps were dominated by the linear inputs, faults and roads. In contrast, the high-gamma maps identified broad regions of hazardous terrain. This discrepancy between quantitative and qualitative results can be explained by the fact that many events reported in the GLC are associated with road closures, leading to a false level of confidence in low-gamma maps that emphasize this feature. Because no single factor (other than slope, which was overlaid separately) is necessary for a landslide to occur, gamma was assigned a value of 0.9, which is consistent with the high values published in several previous studies (Tangestani 2004; Champati ray et al. 2007; Srivastava et al. 2010; Pradhan 2011; dos Santos Alvalá et al. 2013; Ahmed et al. 2014).

4 Results

The landslide susceptibility map is intended to enhance situational awareness with a consistent global picture of mass movements. The map covers the Earth's land surface from 56 South to 72 North latitude (Fig. 4). Each continent evaluated has susceptible areas, but the major mountain chains (Himalayan Arc, Andes, Alps, and Pacific Rim) dominate the map.

In order to assess the map's performance, area under the ROC curve (AUC) was calculated for each landslide inventory. Both classified (5 susceptibility categories) and unclassified (continuous susceptibility values) maps were analyzed to identify any loss of information from classification of the model output into discrete bins (Table 5). Uncertainty from spatial error in the inventories was not analyzed, but only GLC points with an estimated accuracy better than 1 km were used. The AUC for the GLC was 0.82, which indicates a relatively successful classification of terrain (Hosmer and Lemeshow 2005; Beguería 2006). Local performance of the global susceptibility map ranged from very good (Nicaragua) to poor (Badakhshan) (Table 5). Local landslide inventories are typically produced for landslide hotspots. In the context of a global map, the entire study area may

Table 5 Performance of the global susceptibility map was analyzed with eight local landslide inventories

Performance appears to depend upon the specific events recorded in each inventory, not upon the size, terrain, or climate of the study area

Inventory	AUC	
	Unclassified	Classified
Study area		
Global	0.85	0.82
Badakhshan, Afghanistan	0.61	0.59
El Salvador	0.7	0.69
Eastern Guatemala	0.7	0.69
Italy	0.66	0.65
Koshi Basin, Nepal–India–China	0.84	0.82
Nicaragua	0.85	0.83
Oregon, USA	0.75	0.74
Utah, USA	0.82	0.81

be highly susceptible. As a result, a global classification may place nearly all pixels in one category, giving the appearance of randomness in the ROC. AUC values calculated for the classified map were no more than 0.03 lower than for the unclassified fuzzy product, which suggests that the classification process preserved most of the available information.

5 Comparison with previous small-scale maps

The new global landslide susceptibility map resembles previous publications, both in methods and results. Landslide hotspots were identified by Nadim et al. (2006) in many of the same locations that the current study finds highly or very highly susceptible. However, the new map identifies a much larger portion of the world’s surface as highly susceptible than was shown as highly hazardous in the map of landslide and avalanche hotspots. The difference is probably due to the use of a classification system that relies upon “approximate annual frequency” in the prior work. The current study identifies some additional large areas as hotspots, including the Appalachian Mountains in the eastern United States, eastern Brazil, and Madagascar, which were previously classified as “negligible to very low”. This difference is important because many landslides, including fatal ones, have occurred in places like West Virginia, Minas Gerais, and Orissa. The new map also has much in common with the previous global landslide susceptibility map by Hong et al. (2007), including large hotspots in the Andes, Himalaya, and eastern Brazil. The most notable differences are the relatively low susceptibility ratings assigned to Indonesia, the Philippines, and New Zealand by the earlier map. The distribution of categories differs between the maps, with more pixels rated moderately susceptible in the map by Hong et al., and more pixels rated very low in the newer map. The significance of this is that very few areas can be excluded from future analysis on the basis of the older map, whereas the new global map can be used to exclude a majority of the Earth’s land surface from more detailed study. The spatial distribution of fatal landslides (Petley 2012) mostly confirms the patterns seen in all three global maps. Highly rated areas with few fatal landslides, such as the Southern Andes and the Canadian Rockies, tend to be sparsely populated, resulting in fewer reported fatalities.

The landslide susceptibility map of Central America and the Caribbean region (Kirschbaum et al. 2015a) should be very similar to the global map, despite slight differences in methods and data inputs. Since the maps were produced at the same resolution

(30 arc seconds) and with the same number of categories (five), quantitative comparisons were not difficult. First, the susceptibility classes were assigned a numerical value from 1 (very low) to 5 (very high). Then the map of the Caribbean was subtracted from the global map. The global susceptibility ratings were equal to or greater than the prior ratings in almost all locations (Fig. 5). This is attributed to the fact that Central America is a landslide hotspot (Nadim et al. 2006; Petley 2012; Kirschbaum et al. 2015b). While any given location within the region may be relatively less susceptible than other Central American locations, it may be relatively more susceptible than the Earth as a whole. This tendency was also seen in the susceptibility maps associated with the local inventories described above (Table 4). The handful of locations where the Caribbean map indicates higher susceptibility are probably due to the use of an older slope database (Verdin et al. 2007).

The new global map can also be compared to the landslide hazard maps of Indonesia (Cepeda 2010), which have four hazard classes. The hazard map for precipitation-triggered landslides shows the highest hazard in southwestern Sulawesi and western Sumatra, with the lowest hazard in eastern Sumatra and southern Borneo. The hazard map for earthquake-triggered landslides shows the highest hazard in western Sumatra, Morotai, and the mountains of Papua, with the lowest hazard in eastern Sumatra and Borneo. Although it has been subdivided into seismic and meteorological components, this is roughly the same pattern seen in its predecessor, the global map of landslide hotspots (Nadim et al. 2006). The new global map identifies the same locations as highly hazardous, but extends the high and very high classes over much of Indonesia, including eastern Sulawesi and many smaller islands (Fig. 6). Interestingly, both maps portray Java as less hazardous than its neighbors, despite the preponderance of reported landslides. This is probably due to population biases in the landslide inventories, but it might indicate the influence of anthropogenic terrain modification on landslide rates.

Comparison with the European map (Günther et al. 2014) revealed large regional differences (Fig. 7). In particular, the European map shows higher susceptibility in Italy, Ireland, and the United Kingdom, while the global map shows higher susceptibility in Iberia and the Carpathians. The global map shows higher overall susceptibility, which would be expected if Europe were more prone to landslides than the Earth as a whole. Using the European map as a benchmark, the deviation by class is very low: 80%, low:

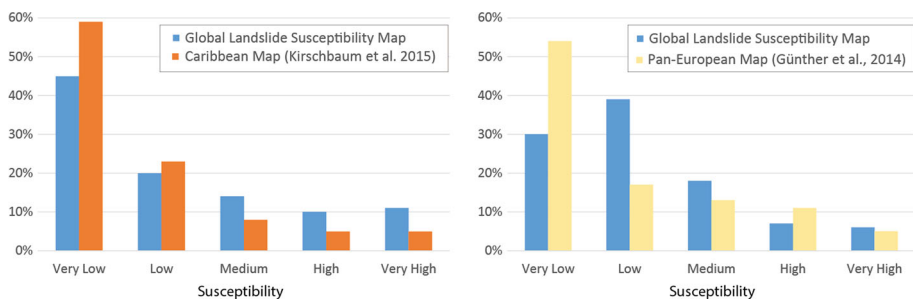


Fig. 5 Relationship between the global landslide susceptibility map and the maps of Europe and the Caribbean. The global map often classified terrain as one category higher than the Caribbean map, but the majority of sites were identical in both maps. Less than 1% of the study area was classified higher by the Caribbean map. The global map exhibited a lower rate of agreement with the European map. In this case, the distribution of higher and lower values was more even. In both cases, the number of large differences between global and regional susceptibility classes was quite small

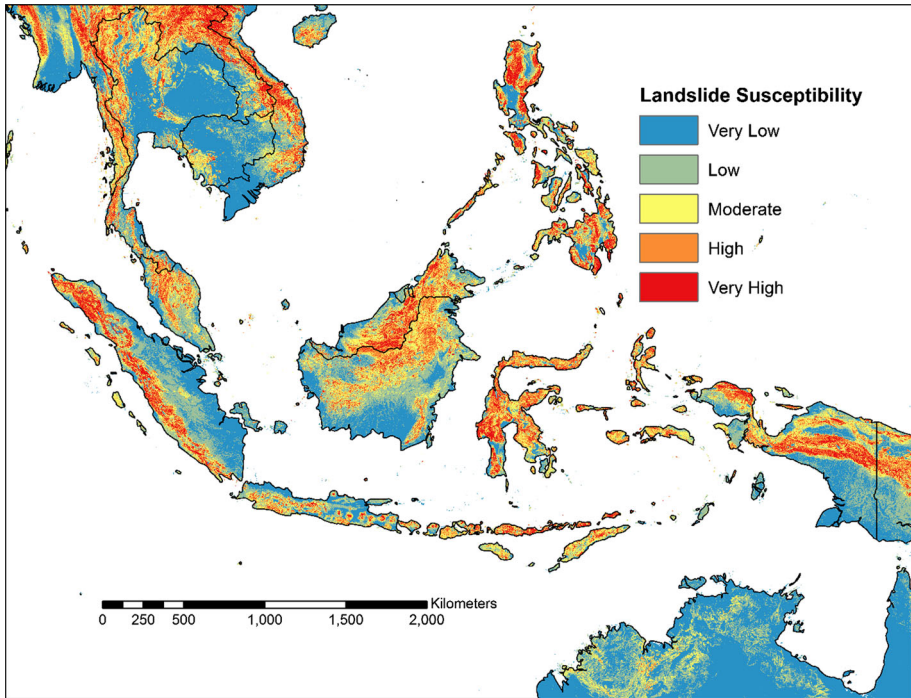


Fig. 6 Fuzzy landslide susceptibility in Indonesia

–56%, moderate: –28%, high: 57%, very high: –17% (Fig. 5). It is interesting to note that although the methods for defining susceptibility classes were quite different, the overall distribution of European land among classes resembles the global map as a whole. The same is not true of landslides (Fig. 3); the better validation of the European susceptibility model can be attributed to the use of better lithological data, larger and more spatially precise landslide inventories, and a more homogeneous study area. Nevertheless, the European map largely confirms the output of the global susceptibility model. Less than 0.2% of the map showed a difference of 4 classes (e.g., a complete inversion from very low to very high), less than 2% of the map showed a difference of 3 or more classes, and less than 11% of the map showed a difference of 2 or more classes. In other words, there was no difference in 45% of the pixels, and the maps differed by a single class in another 45% of the pixels.

This comparison suggests that maps produced with different methods, data, and scope may show largely similar results. However, maps focused on specific landslide hotspots are not directly comparable to broader overviews unless a single, rigorous classification method was applied to both maps.

6 Discussion

While comparison with previous small-scale maps revealed strong similarities, this global landslide susceptibility map improves upon prior maps in four important ways. First, several new or updated datasets have been released in the last decade. In the current

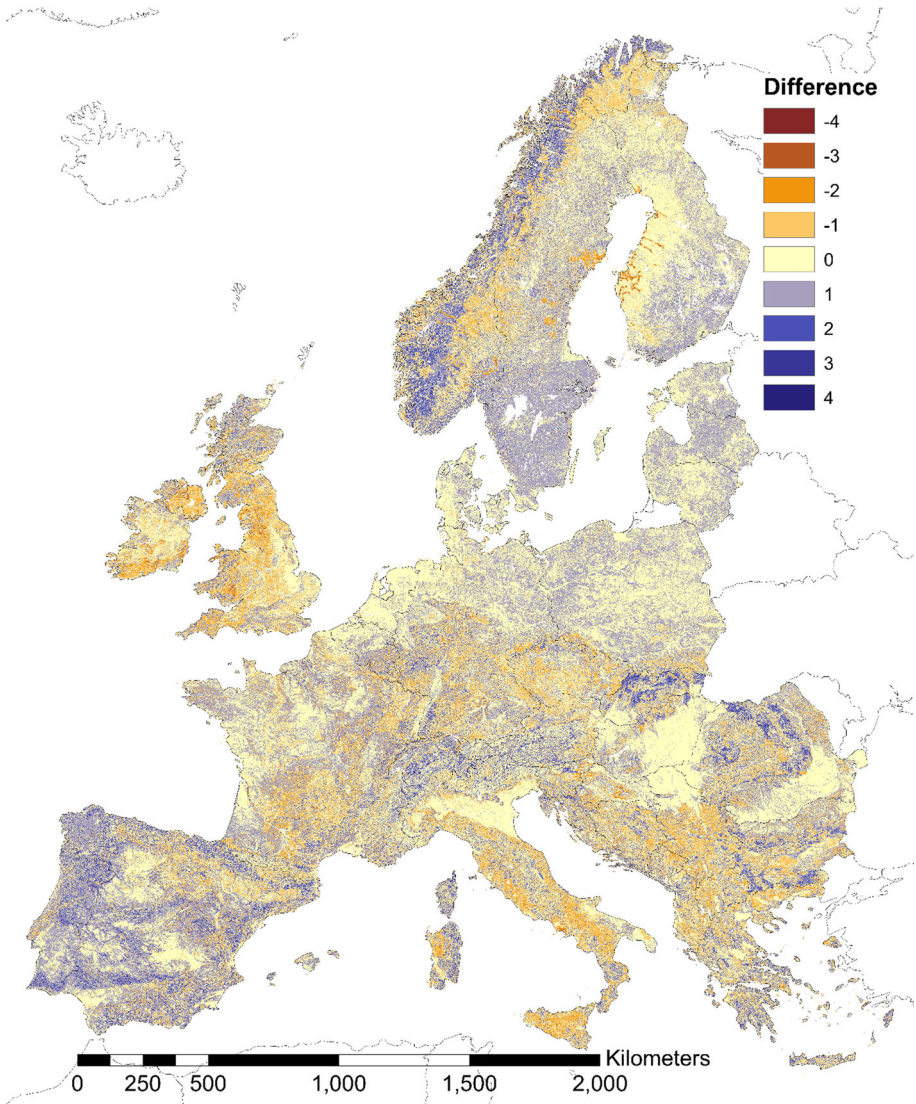


Fig. 7 New global landslide susceptibility map and the European map (Günther et al. 2014) were assigned integer values from 1 (very low susceptibility) to 5 (very high). The European map was then subtracted from the global map, so positive values indicate areas where the global map has higher susceptibility and negative indicates where the European map is higher. Numerous differences between the global and European landslide susceptibility maps can be seen. The European map exceeds the global map over large portions of Great Britain and Ireland (*brown*). The global map shows higher landslide susceptibility in most of Portugal and Spain (*purple*)

context, the most important of these is a DEM made with high-quality SRTM void-filling techniques. Second, the use of a conservative method for aggregating 90-m slope values means that all major topographic features were considered by this analysis. Third, the use of fuzzy overlay preserves the full information content of continuous variables like slope gradient. Fourth, the simple classification scheme will be familiar to users of other

susceptibility maps, but the uneven pixel distribution should draw the user's attention to the most critical sites.

Nevertheless, several features of the new map may limit its use. First, the resolution of the map is approximately 1 km, and terrain varies significantly within many pixels. The choice to aggregate slope by computing the maximum value means that some pixels may contain a very small area of steep terrain, while the remainder is not susceptible to landslides. Second, the use of biased and incomplete landslide inventories to evaluate the susceptibility map makes the results more difficult to interpret. Although this susceptibility model (Fig. 2) was not fitted empirically, landslide inventories informed the prior research on which it was based. Third, the Geological Map of the World is only appropriate for use over very large areas. At local and national scales, more detailed information is often available, but varies in quality, format, and cost. Fourth, this map models all mass movements with the same treatment. The real world is more complex, and factors which drive rock toppling in Canada are not the same as those which can cause debris flows in New Guinea. Fifth, this map does not provide an explicit hazard level in the form of an annual probability of slope failure. Therefore, it is very likely that landslides will occur at some date in all of the very highly susceptible locations, but the size, frequency, and timing of those events are not known. These limitations suggest that the global susceptibility map is best used for a few purposes: situational awareness of global landslide hotspots and potential occurrence, the development of global decision support systems, and prioritization of future landslide research. It is not appropriate for decisions about infrastructure design, building code legislation, or local land-use planning.

Excerpts from this landslide susceptibility map have already been used during the period leading up to potential disasters. In one such instance, the approach of Hurricane Madeline toward the Hawaiian Islands triggered a request for information on the potential for landslides. Although the global map is not tailored specifically to this location, it was still the most relevant and detailed dataset available to decision makers. This map has also been applied as one component of a global landslide nowcast system (Kirschbaum and Stanley 2016). The nowcasts are issued at two levels, high-hazard and moderate-hazard, which correspond to different classes of the global susceptibility map. After considering susceptibility, a 7-day antecedent rainfall index is compared to historical precipitation levels to identify hazardous locations in nearly real time. While this system focuses upon rain, other landslide triggers, such as melting snow or recent seismicity, could be considered in similar models.

7 Conclusions

This research assessed landslide susceptibility at a resolution of approximately 1 km with nearly global coverage. The map was evaluated with one Global Landslide Catalog and several local to regional landslide inventories. The geographic distribution of landslide susceptibility is very similar to that in previous small-scale maps, with the most dangerous terrain located around the Pacific Rim and along the Himalayan Mountains. Other hot spots can be found in Europe, Africa, and the Americas. While this map benefited from several excellent and free datasets, further improvements to thematic data, particularly in soil mapping of mountain regions and landslide cataloging, would improve the results of any future work. The global susceptibility map might be improved by incorporation of any future in situ and satellite-based datasets with improved resolution, accuracy, or

completeness. The map may be useful for long-term risk assessment and disaster response planning, as well as in the development of real-time hazard models.

Acknowledgements Thank you to all of the contributors to the Global Landslide Catalog since its creation in 2007. Thank you also to all of those who provided landslide inventories for analysis, including Deo Raj Gurung and Jianqiang Zhang (ICIMOD), Mauro Rossi (CNR IRPI), Graziella Devoli, Manuel Diaz (MARN), the Oregon DOGAMI, the USGS, and the Utah Geological Survey. This work was supported by NASA's Precipitation Measurement Missions.

References

- Ahmed MF, Rogers JD, Ismail EH (2014) A regional level preliminary landslide susceptibility study of the upper Indus river basin. *Eur J Remote Sens* 47:343–373. doi:[10.5721/EuJRS20144721](https://doi.org/10.5721/EuJRS20144721)
- Ayalew L, Yamagishi H (2005) The application of GIS-based logistic regression for landslide susceptibility mapping in the Kakuda-Yahiko Mountains, Central Japan. *Geomorphology* 65:15–31. doi:[10.1016/j.geomorph.2004.06.010](https://doi.org/10.1016/j.geomorph.2004.06.010)
- Beguieria S (2006) Changes in land cover and shallow landslide activity: a case study in the Spanish Pyrenees. *Geomorphology* 74:196–206. doi:[10.1016/j.geomorph.2005.07.018](https://doi.org/10.1016/j.geomorph.2005.07.018)
- Bhatt BP, Awasthi KD, Heyojoo BP et al (2013) Using geographic information system and analytical hierarchy process in landslide hazard zonation. *Appl Ecol Environ Sci* 1:14–22. doi:[10.12691/aees-1-2-1](https://doi.org/10.12691/aees-1-2-1)
- BMTPC (Building Materials and Technology Promotion Council Ministry of Urban Development and Poverty Alleviation Government of India), CDMM (Centre for Disaster Mitigation and Management, Anna University) (2003) *Landslide Hazard Zonation Atlas of India*. New Delhi
- Bonham-Carter G (1994) *Geographic information systems for geoscientists: modelling with GIS*. Elsevier, Amsterdam
- Bouysse P (2009) *Geological map of the world at 1:50 000 000*. Commission for the Geological Map of the World
- Brabb EE, Colgan JP, Best TC (1999) Map showing inventory and regional susceptibility for Holocene debris flows and related fast moving landslides in the conterminous United States. Accessed <http://pubs.usgs.gov/mf/1999/2329/>
- Bucknam RC, Coe JA, Chavarria MM et al (2001) Landslides triggered by Hurricane Mitch in Guatemala—inventory and discussion. US Geological Survey Open File Report 01-443:38
- Center for International Earth Science Information Network, Information Technology Outreach Services (2013) Global roads open access data set, version 1. <http://sedac.ciesin.columbia.edu/data/set/global-roads-open-access-v1>. Accessed 1 Jan 2015
- Cepeda J, Smebye, H, Vangelsten, B et al (2010) *Landslide risk in Indonesia. Global assessment report on disaster risk reduction*. United Nations
- Champati ray PK, Dimri S, Lakhera RC, Sati S (2007) Fuzzy-based method for landslide hazard assessment in active seismic zone of Himalaya. *Landslides* 4:101–111. doi:[10.1007/s10346-006-0068-6](https://doi.org/10.1007/s10346-006-0068-6)
- Dahal RK, Hasegawa S, Nonomura A et al (2008) Predictive modelling of rainfall-induced landslide hazard in the Lesser Himalaya of Nepal based on weights-of-evidence. *Geomorphology* 102:496–510. doi:[10.1016/j.geomorph.2008.05.041](https://doi.org/10.1016/j.geomorph.2008.05.041)
- de Ferranti J (2014a) Digital Elevation Data—with SRTM voids filled using accurate topographic mapping. <http://www.viewfinderpanoramas.org/dem3.html>. Accessed 17 Nov 2015
- de Ferranti J (2014b) Digital Elevation Data: SRTM void fill. <http://viewfinderpanoramas.org/voidfill.html>. Accessed 19 May 2016
- Devoli G, Morales A, Høeg K (2007a) Historical landslides in Nicaragua—collection and analysis of data. *Landslides* 4:5–18. doi:[10.1007/s10346-006-0048-x](https://doi.org/10.1007/s10346-006-0048-x)
- Devoli G, Strauch W, Chávez G, Høeg K (2007b) A landslide database for Nicaragua: a tool for landslide-hazard management. *Landslides* 4:163–176. doi:[10.1007/s10346-006-0074-8](https://doi.org/10.1007/s10346-006-0074-8)
- DOGAMI (Oregon Department of Geology and Mineral Industries) (2015) SLIDO: statewide landslide information layer for Oregon. <http://www.oregongeology.org/sub/slido/data.htm>. Accessed 11 Oct 2015
- dos Santos Alvalá RC, Camarinha PIM, Canavesi V (2013) Landslide susceptibility mapping in the coastal region in the State of São Paulo, Brazil. In: American Geophysical Union, Spring Meeting

- Elliott AH, Hartly KM (2010) Landslide maps of Utah. Utah Geological Survey Map 246DM:14. 46 plates. 1:100,000 scale. DVD
- ESRI (2013) ArcGIS Desktop, version 10.2. Environmental Systems Research Institute, Redlands, California
- Frolova JV, Gvozdeva IP, Kuznetsov NP (2015) Effects of Hydrothermal Alterations on Physical and Mechanical Properties of Rocks in the Geysers Valley (Kamchatka Peninsula) in Connection with Landslide Development. In: Proceedings World Geothermal Congress 2015, pp 1–6
- Gerencia de Geología (2012) Landslide inventory of El Salvador. Ministerio de Medio Ambiente y Recursos Naturales, El Salvador
- Günther A, Van Den Eeckhaut M, Malet J-P et al (2014) Climate-physiographically differentiated Pan-European landslide susceptibility assessment using spatial multi-criteria evaluation and transnational landslide information. *Geomorphology* 224:69–85. doi:[10.1016/j.geomorph.2014.07.011](https://doi.org/10.1016/j.geomorph.2014.07.011)
- Guzzetti F, Cardinali M, Reichenbach P (1994) The AVI project: a bibliographical and archive inventory of landslides and floods in Italy. *Environ Manag* 18:623–633. doi:[10.1007/BF02400865](https://doi.org/10.1007/BF02400865)
- Haigh MJ, Rawat JS, Bartarya SK (1989) Environmental indicators of landslide activity along the Kilbury road, Nainital, Kumaun lesser Himalaya. *Mt Res Dev* 9:25–33
- Haigh MJ, Rawat JS, Rawat MS et al (1995) Interactions between forest and landslide activity along new highways in the Kumaun Himalaya. *For Ecol Manag* 78:173–189
- Hansen MC, Potapov PV, Moore R et al (2013) High-resolution global maps of 21st-century forest cover change. *Science* 342:850–853. doi:[10.1126/science.1244693](https://doi.org/10.1126/science.1244693)
- Haque U, Blum P, da Silva PF et al (2016) Fatal landslides in Europe. *Landslides*. doi:[10.1007/s10346-016-0689-3](https://doi.org/10.1007/s10346-016-0689-3)
- Hijmans RJ (2015) Raster: geographic data analysis and modeling. R package version 2.4-15. <https://CRAN.R-project.org/package=raster>
- Hirano A, Welch R, Lang H (2003) Mapping from ASTER stereo image data: DEM validation and accuracy assessment. *ISPRS J Photogramm Remote Sens* 57:356–370. doi:[10.1016/S0924-2716\(02\)00164-8](https://doi.org/10.1016/S0924-2716(02)00164-8)
- Hong Y, Adler RF, Huffman G (2007) Use of satellite remote sensing data in the mapping of global landslide susceptibility. *Nat Hazards* 43:245–256. doi:[10.1007/s11069-006-9104-z](https://doi.org/10.1007/s11069-006-9104-z)
- Hosmer DW, Lemeshow S (2005) Assessing the fit of the model. In: *Applied logistic regression*, 2nd edn. Wiley, Inc., Hoboken, NJ, USA, pp 143–202
- ICIMOD (International Centre for Integrated Mountain Development) (1992) Landslides in Koshi River Basin of 1990. <http://rds.icimod.org/Home/DataDetail?metadatald=23175&searchlist=True>. Accessed 7 Jan 2015
- ICIMOD (International Centre for Integrated Mountain Development) (2010) Landslides in Koshi River Basin of 2010. <http://rds.icimod.org/Home/DataDetail?metadatald=23176&searchlist=True>. Accessed 7 Jan 2015
- Jarvis A, Reuter H, Nelson A, Guevara E (2008) Hole-filled SRTM for the globe version 4. Available from the CGIAR-CSI SRTM 90 m Database
- Jezek KC (2002) RADARSAT-1 Antarctic mapping project: change-detection and surface velocity campaign. *Ann Glaciol* 34:263–268. doi:[10.3189/172756402781818030](https://doi.org/10.3189/172756402781818030)
- Keefer DK (1994) The importance of earthquake-induced landslides to long-term slope erosion and slope-failure hazards in seismically active regions. *Geomorphology* 10:265–284. doi:[10.1016/0169-555X\(94\)90021-3](https://doi.org/10.1016/0169-555X(94)90021-3)
- Kirschbaum DB, Adler RF, Hong Y et al (2010) A global landslide catalog for hazard applications: method, results, and limitations. *Nat Hazards* 52:561–575. doi:[10.1007/s11069-009-9401-4](https://doi.org/10.1007/s11069-009-9401-4)
- Kirschbaum D, Stanley T (2016) A satellite-based global landslide hazard assessment model for situational awareness. In: *Geological society of america abstracts with programs*, vol 48. doi:[10.1130/abs/2016AM-279271](https://doi.org/10.1130/abs/2016AM-279271)
- Kirschbaum DB, Stanley T, Yatheendradas S (2015a) Modeling landslide susceptibility over large regions with fuzzy overlay. *Landslides*. doi:[10.1007/s10346-015-0577-2](https://doi.org/10.1007/s10346-015-0577-2)
- Kirschbaum DB, Stanley T, Zhou Y (2015b) Spatial and temporal analysis of a global landslide catalog. *Geomorphology* 249:4–15. doi:[10.1016/j.geomorph.2015.03.016](https://doi.org/10.1016/j.geomorph.2015.03.016)
- Korup O, Stolle A (2014) Landslide prediction from machine learning. *Geol Today* 30:26–33. doi:[10.1111/gto.12034](https://doi.org/10.1111/gto.12034)
- Larsen IJ, Montgomery DR (2012) Landslide erosion coupled to tectonics and river incision. *Nat Geosci* 5:468–473. doi:[10.1038/ngeo1479](https://doi.org/10.1038/ngeo1479)
- Larsen MC, Parks JE (1997) How wide is a road? The association of roads and mass-wasting in a forested montane environment. *Earth Surf Process Landf* 22:835–848. doi:[10.1002/\(SICI\)1096-9837\(199709\)22:9<835::AID-ESP782>3.0.CO;2-C](https://doi.org/10.1002/(SICI)1096-9837(199709)22:9<835::AID-ESP782>3.0.CO;2-C)

- Lehner B, Verdin K, Jarvis A (2008) New global hydrography derived from spaceborne elevation data. *EOS Trans Am Geophys Union* 89:93. doi:[10.1029/2008EO100001](https://doi.org/10.1029/2008EO100001)
- Liu C, Li W, Wu H et al (2013) Susceptibility evaluation and mapping of China's landslides based on multi-source data. *Nat Hazards* 69:1477–1495. doi:[10.1007/s11069-013-0759-y](https://doi.org/10.1007/s11069-013-0759-y)
- Nadim F, Kjekstad O, Peduzzi P et al (2006) Global landslide and avalanche hotspots. *Landslides* 3:159–173. doi:[10.1007/s10346-006-0036-1](https://doi.org/10.1007/s10346-006-0036-1)
- NIMA (National Imagery and Mapping Agency) (1993) Vector map (VMap) level 0. <http://earth-info.nga.mil/publications/vmap0.html>. Accessed 1 Jan 2014
- Okamoto T, Sakurai M, Tsuchiya S (2013) Secondary hazards associated with coseismic landslide. In: Ugai K, Yagi H, Wakai A (eds) *Earthquake-induced landslides*. Springer, Berlin, pp 77–82
- OpenStreetMap contributors (2015) OpenStreetMap. <http://osm-x-tractor.org/Data.aspx>. Accessed 7 Jun 2015
- Petley DN (2012) Global patterns of loss of life from landslides. *Geology* 40:927–930. doi:[10.1130/G33217.1](https://doi.org/10.1130/G33217.1)
- Petley DN, Dunning SA, Rosser NJ (2005) The analysis of global landslide risk through the creation of a database of worldwide landslide fatalities. In: Hungr O, Fell R, Couture R, Eberhardt E (eds) *Landslide risk management*. CRC Press, Boca Raton, p 776
- Petley DN, Hearn GJ, Hart A et al (2007) Trends in landslide occurrence in Nepal. *Nat Hazards* 43:23–44. doi:[10.1007/s11069-006-9100-3](https://doi.org/10.1007/s11069-006-9100-3)
- Pradhan B (2011) Use of GIS-based fuzzy logic relations and its cross application to produce landslide susceptibility maps in three test areas in Malaysia. *Environ Earth Sci* 63:329–349. doi:[10.1007/s12665-010-0705-1](https://doi.org/10.1007/s12665-010-0705-1)
- Rabus B, Eineder M, Roth A, Bamler R (2003) The shuttle radar topography mission—a new class of digital elevation models acquired by spaceborne radar. *ISPRS J Photogramm Remote Sens* 57:241–262. doi:[10.1016/S0924-2716\(02\)00124-7](https://doi.org/10.1016/S0924-2716(02)00124-7)
- Radbruch-Hall DH, Colton RB, Davies WE et al (1982) *Landslide overview map of the conterminous United States*. U.S Government Printing Office, Washington
- Regmi AD, Devkota KC, Yoshida K et al (2013) Application of frequency ratio, statistical index, and weights-of-evidence models and their comparison in landslide susceptibility mapping in Central Nepal Himalaya. *Arab J Geosci* 7:725–742. doi:[10.1007/s12517-012-0807-z](https://doi.org/10.1007/s12517-012-0807-z)
- Reid ME, Sisson TW, Brien DL (2001) Volcano collapse promoted by hydrothermal alteration and edifice shape, Mount Rainier, Washington. *Geology* 29:779. doi:[10.1130/0091-7613\(2001\)029<0779:VCPBHA>2.0.CO;2](https://doi.org/10.1130/0091-7613(2001)029<0779:VCPBHA>2.0.CO;2)
- Rubel Y, Ahmed B (2013) Understanding the issues involved in urban landslide vulnerability in Chittagong metropolitan area. *Association of American Geographers (AAG), Bangladesh*
- Scheidegger AE, Ai NS (1986) Tectonic processes and geomorphological design. *Tectonophysics* 126:285–300. doi:[10.1016/0040-1951\(86\)90234-9](https://doi.org/10.1016/0040-1951(86)90234-9)
- Schutz BE, Zwally HJ, Shuman CA et al (2005) Overview of the ICESat mission. *Geophys Res Lett* 32:L21S01. doi:[10.1029/2005GL024009](https://doi.org/10.1029/2005GL024009)
- Sidle RC, Pearce AJ, O'Loughlin CL (1985) Effects of land management on soil mass movement. In: Sidle RC, Pearce AJ, O'Loughlin CL (eds) *Hillslope stability and land use*. American Geophysical Union, Washington, pp 73–88
- Sidle RC, Ziegler AD, Negishi JN et al (2006) Erosion processes in steep terrain—truths, myths, and uncertainties related to forest management in Southeast Asia. *For Ecol Manag* 224:199–225. doi:[10.1016/j.foreco.2005.12.019](https://doi.org/10.1016/j.foreco.2005.12.019)
- Srivastava V, Srivastava HB, Lakhera RC (2010) Fuzzy gamma based geomatic modelling for landslide hazard susceptibility in a part of Tons river valley, northwest Himalaya, India. *Geomat Nat Hazards Risk* 1:225–242. doi:[10.1080/19475705.2010.490103](https://doi.org/10.1080/19475705.2010.490103)
- Steger S, Brenning A, Bell R et al (2016a) Exploring discrepancies between quantitative validation results and the geomorphic plausibility of statistical landslide susceptibility maps. *Geomorphology* 262:8–23. doi:[10.1016/j.geomorph.2016.03.015](https://doi.org/10.1016/j.geomorph.2016.03.015)
- Steger S, Brenning A, Bell R, Glade T (2016b) The impact of systematically incomplete and positionally inaccurate landslide inventories on statistical landslide susceptibility models. In: *EGU general assembly conference abstracts* 18:6666
- Tangestani MH (2004) Landslide susceptibility mapping using the fuzzy gamma approach in a GIS, Kakan catchment area, southwest Iran. *Aust J Earth Sci* 51:439–450. doi:[10.1111/j.1400-0952.2004.01068.x](https://doi.org/10.1111/j.1400-0952.2004.01068.x)
- USGS (United States Geological Survey) (2008) *Global land survey digital elevation model*. Global Land Cover Facility, University of Maryland, College Park, Maryland. <http://glcf.umd.edu/data/glsdem/>
- van Westen CJ, Castellanos E, Kuriakose SL (2008) Spatial data for landslide susceptibility, hazard, and vulnerability assessment: an overview. *Eng Geol* 102:112–131. doi:[10.1016/j.enggeo.2008.03.010](https://doi.org/10.1016/j.enggeo.2008.03.010)

- Verdin KL, Godt JW, Funk C et al (2007) Development of a global slope dataset for estimation of landslide occurrence resulting from earthquakes: U.S. Geological Survey, Colorado. Open-File Report 2007–1188:25
- Weirich F, Blesius L (2007) Comparison of satellite and air photo based landslide susceptibility maps. *Geomorphology* 87:352–364. doi:[10.1016/j.geomorph.2006.10.003](https://doi.org/10.1016/j.geomorph.2006.10.003)
- Zhang J, Gurung DR, Liu R et al (2015) Abe Barek landslide and landslide susceptibility assessment in Badakhshan Province, Afghanistan. *Landslides* 12:597–609. doi:[10.1007/s10346-015-0558-5](https://doi.org/10.1007/s10346-015-0558-5)
- Zweig MH, Campbell G (1993) Receiver-operating characteristic (ROC) plots: a fundamental evaluation tool in clinical medicine. *Clin Chem* 39:561–577